This document is confidential and is proprietary to the American Chemical Society and its authors. Do not copy or disclose without written permission. If you have received this item in error, notify the sender and delete all copies.

Vibration Assisted Intersystem Crossing in the Ultrafast Excited-State Relaxation Dynamics of Halo-Coumarins

Journal:	The Journal of Physical Chemistry
Manuscript ID	jp-2021-08489g.R2
Manuscript Type:	Special Issue Article
Date Submitted by the Author:	n/a
Complete List of Authors:	Das, Aritra; Indian Institute of Technology Kanpur, Department of Chemistry Ghosh, Sujit Kumar; University of Miami Ramamurthy, Vaidhyanathan; University of Miami, Chemistry; Sen, Pratik; Indian Institute of Technology Kanpur, Department of Chemistry

SCHOLARONE™ Manuscripts

Vibration Assisted Intersystem Crossing in the Ultrafast Excited-State Relaxation Dynamics of Halo-Coumarins

Aritra Das, Sujit Kumar Ghosh, Vaidhyanathan Ramamurthy*, and Pratik Sen*, Sen

§Department of Chemistry, Indian Institute of Technology Kanpur, Kanpur – 208 016, UP, India

[†]Department of Chemistry, University of Miami, Coral Gables – 33146, Florida, USA

Abstract

Due to its numerous applications, triplet formation and resulting phosphorescence remain a frontier area of research for over eight decades. Facile intersystem crossing (ISC) is the primary requirement for triplet formation and observation of phosphorescence. Incorporation of heavy atom in molecules is one of the common approaches employed to facilitate ISC. A detailed study of the excited state dynamics that governs ISC is necessary to understand the mechanism of heavy atom effect (HAE). Incorporation of iodine at the 3 position of coumarin-1 reduces fluorescence quantum yield (ϕ_f) drastically as expected, whereas bromine substitution at the same position increased the ϕ_f . Such a contrasting effect of the two heavy atoms suggests that there are other features yet to be discovered to fully understand the HAE. Detailed steady state and femtosecond transient absorption studies along with theoretical calculations suggest that the C3-X (X=Br, I) bond vibration plays an important role in the ISC process. The study reveals that while in the case of the iodo-derivative there is no energy barrier in the singlet triplet crossing path, there is a barrier in the case of bromoderivative, which slows the ISC process. Such an unexpected phenomenon is not limited to halocoumarins as this rationalizes the photobehavior of 1-bromo/iodo substituted naphthalenes as well.

Key words: Intersystem crossing, Heavy atom effect, Vibration, Phosphorescence, Halocoumarin

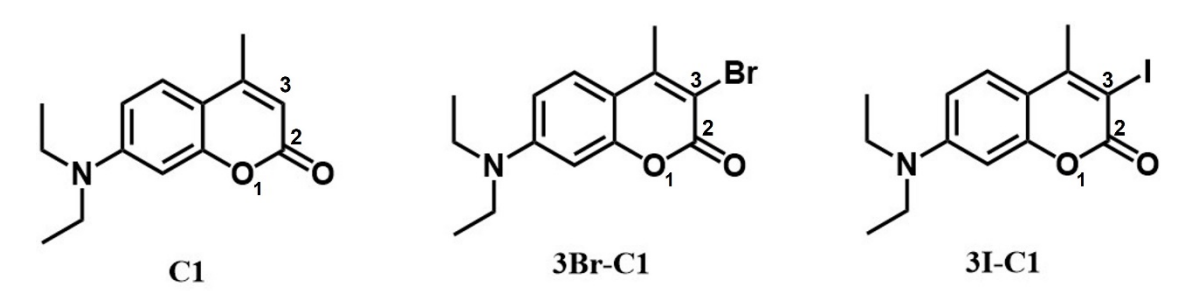
Introduction:

Recent intense research on phosphorescence¹⁻⁵ could be traced to G. N. Lewis' statement to his student in 1942 namely, "You know, those triplet states that Mulliken was talking about in ethylene are probably the phosphorescent state". 6 The experimental evidence for the existence of triplet states in phosphorescent materials by Kasha and Lewis in 1944 also revealed the importance of intersystem crossing (ISC) through spin-orbit coupling (SOC).⁷⁻⁹ The observation of heavy atom effect on phosphorescence by McClure in 1949 and the quadratic dependence of the SOC with the atomic number ($\propto Z^4$) found handy to tune the phosphorescence property of a system.¹⁰⁻¹² Halogen substitution in organic molecules like naphthalene, azulene, phenanthrene, quinoline, quinoxaline and anthracene is a preferred way to introduce heavy atom effect in the past. 10-22 A change in orbital type from $\pi\pi^* \to n\pi^*$ or $n\pi^* \to \pi\pi^*$ has also been noted to facilitate ISC through stronger SOC (El Sayed rule).²³ However, El Sayed rule only considers the electronic aspect of the transition and ignores the vibrational component.²⁴ Depending on the extent of nuclear geometry difference between the singlet and triplet states, there can be two regimes of ISC.²⁵ When the difference between singlet and triplet geometries is small, it falls in the small coupling regime and the rate of ISC decreases exponentially with increasing energy gap (ΔE) between the two states.²⁶⁻²⁷ On the other hand, when the geometries of the singlet and triplet states differ significantly and their surfaces cross, it falls in the strong coupling regime and ISC rate constant follows a bell-shaped dependence with ΔE . This has similarity to the bell-shaped dependence described in the Marcus theory for electron transfer.²⁶⁻²⁷ If this is true, it should be possible to prove the applicability of Marcus theory for ISC in the strong coupling regime. In this context we note that there are reports of facile ISC without heavy atom effect, where crossing between singlet and triplet states is present.^{24,27}

The ISC trend of 1-halonaphthalene is an example in support of the idea that SOC is not the only factor that controls the ISC from excited singlet to the triplet. The ratio of the square of SOC constants for 1-bromo and 1-iodonaphthalene is 1:4.2, whereas, the ratio of their ISC rate constants is measured to be 1:9.3. 10,12 The 2.2 times larger value of the ISC for 1-iodonaphthalene than the predicted value based on SOC suggests the involvement of other factor(s) associated with the heavy atom incorporation, which remains mostly unexplored. When the excited state is non-adiabatic in nature, we cannot consider the spin, electronic and vibrational contributions separately. In such cases, the ISC cannot be described solely in terms of conventional SOC values and a change in the nuclear geometry may also dictate the

course of relaxation following the photoexcitation. In general, vibration is likely to be important for an excited state process, which may also be the case in the singlet-triplet ISC process. Such examples are known: in the case of inorganic materials and metal complexes, such a phenomenon has been reported.²⁸⁻³¹ For example, in [Fe(bpy)3]²⁺ the singlet triplet transfer occurs along the Fe-N distance coordinate.²⁸ Similarly, in Re(L)(CO)₃⁻ the ISC is non-adiabatic in nature and coupled with the complex's low-frequency vibrational modes.²⁹ Similar vibronic involvement in ISC was speculated in cases of PtPOP-BF₂ and transition-metal trifluoride compounds like MnF₃ and CoF₃.³⁰⁻³¹ Quantum dynamics simulation also predicted the role of prefulvene normal mode of benzene in ISC.³²⁻³⁴ Another important report in this direction is the ISC of a xanthone derivative, where spin mixing has been observed along the C=O elongation coordinate.³⁵

The above examples prompted us to probe this phenomenon further employing halogen substituted 7-diethylamino-4-methylcoumarins as probe molecules (Scheme 1). If the C–X vibration plays a role in ISC, the HAE would be expected to be position dependent. To explore this, we carried out femtosecond transient absorption spectroscopic experiments and quantum chemical calculations with two halogen substituted 7-diethylamino-4-methylcoumarins as examples. Results suggest that the ISC rate is dictated by the carbon-halogen bond vibration. We have extrapolated the above conclusions to halonaphthalenes.



Scheme 1. Molecular structures of coumarin 1 (C1), 3-bromo-coumarin 1 (3Br-C1) and 3-iodo-coumarin 1 (3I-C1).

Methods:

Materials: Coumarin 1 (C1, Exciton Inc., USA) wase used as received. The synthesis and characterization of 3-bromo-coumarin 1 (3Br-C1) and 3-iodo-coumarin 1 (3I-C1) are described in the section S1 of the SI. Naphthalene (Nap), 1-bromonaphthalene (1Br-Nap) and 2-bromonaphthalene (2Br-Nap) were purchased from Avra Synthesis Pvt. Ltd. and used after recrystallization. Octa acid (OA) was synthesized, purified and characterized following the published procedure.³⁶⁻³⁸ Spectroscopic grade methanol (MeOH) and cyclohexane (CHX)

(Fisher Scientific, India) were used after distillation. Double distilled water was used throughout the study.

Experimental: Absorption spectra were recorded on a commercial spectrophotometer (UV-2450, Shimadzu, Japan) and emission spectra were recorded on commercial fluorimeter (FluoroMax-4, Jobin Yvon, USA). The characterization and nature of complex were carried out by Bruker 400/500 MHz ¹H NMR. Femtosecond time resolved data were acquired on a commercial transient absorption spectrometer (FemtoFrame-II, IB Photonics, Bulgaria). The details of the setup are described earlier³⁹⁻⁴¹ and only a brief overview is presented here. The fundamental 800 nm light was obtained from a Ti-Sapphire regenerative amplifier (Spitfire Pro XP, Spectra-Physics, USA) pumped by a 20-W Q-switched Nd:YLF laser (Empower, Spectra-Physics, USA) and seeded with a Ti-Sapphire femtosecond oscillator (MaiTai SP, Spectra-Physics, USA). The fundamental light thus obtained was divided into two parts. One part was passed through a β-barium borate crystal to generate the 400 nm light, which was used as pump pulse. The other part of the beam was passed through a delay stage and focused on a sapphire crystal to generate the white light continuum, which was used as the probe light. After passing through the sample the probe light was dispersed in polychromator and detected using a CCD. The power of the pump light was kept $\sim 10 \mu W$. The pulse width of the fundamental light was 80 fs and the instrument response function was measured to be 150 fs.

Theoretical studies: Density functional theory (DFT) calculations were performed with Gaussian 09 package.⁴² We used the B3LYP exchange correlation functional and 6-311++G (d,p) basis set for C, H, N, O and LANL2DZ basis set for Br and I for the DFT calculations. The molecule was optimized in methanol using PCM model, followed by frequency calculations to visualize the corresponding normal modes of vibrations and TD-DFT calculation to calculate the absorption wavelengths. We applied TD-DFT method to determine the vertical transition energies from the ground electronic state (S₀) to the higher electronic states and thus constructed the potential energy curves (PEC) for different electronic states in methanol. To check the effect of SOC on the PEC, we have used Orca 4.2.1 package.⁴³ B3LYP exchange correlation functional and def2-TZVP basis set was used for the SOC-corrected TD-DFT calculations.

Results:

Steady state and TCSPC experiments

In scheme 1 the molecular structures of three coumarins used in this work are provided. The steady state absorption and emission spectra of the coumarins in methanol (MeOH) and cyclohexane (CHX) (see figure S1 of the SI) are included as figure S1(see SI). The absorption and emission maxima with the calculated Stokes shifts in different solvents for the three coumarins are tabulated in table 1. All the halo-derivatives showed expected solvatochromic properties based on the behavior of the parent coumarin (C1). The fluorescence quantum yields (ϕ_f) of these coumarins were estimated in different solvents (see table 1) using C1@ MeOH or C1@CHX as the standard.⁴⁴ The average fluorescence lifetimes of these three molecules were recorded using TCSPC method. The results are consolidated in table 1.

Table 1. Steady state absorption and emission parameters with average fluorescence lifetimes of coumarin 1 (C1), 3-bromo-coumarin 1 (3Br-C1) and 3-iodo-coumarin 1 (3I-C1) in methanol (MeOH) and cyclohexane (CHX).

Dye	Solvent	λ_{max}^{abs} (nm)	λ_{max}^{em} (nm)	Stokes shift (nm)	ϕ_f (%)	$ au_{avg}$ (ns)
C1	MeOH	374.6	450	75.4	37.5	2.07
3Br-C1		387.0	471	84.0	47.6	2.46
3I-C1		391.1	455	64.1	2.6	1.69
C1	CHX	350.6	391	40.4	49.0	2.54
3Br-C1		364.8	410	45.2	55.3	2.59
3I-C1		369.6	393	23.4	15.3	2.43

Table 2. Time constants obtained from the global fitting of the transient absorption spectra (pump: 400 nm; probe: 470-750 nm) of coumarin 1 (C1), 3-bromo-coumarin 1 (3Br-C1) and 3-iodo-coumarin 1 (3I-C1) in methanol (MeOH).

Dye	$ au_1(ps)$	$ au_2(\mathrm{ps})$	$ au_3(ext{ns})$	
C1	3.2	10.3	2.04	
3Br-C1	0.9	12.6	2.14	
3I-C1	0.9	61.8	2.00	

Transient absorption spectroscopy

The femtosecond transient absorption (TA) spectroscopic study of C1, 3Br-C1 and 3I-C1 were performed in methanol. The TA spectra of C1, 3Br-C1 and 3I-C1 in methanol consist of stimulated emission (SE) bands respectively around 470 nm, 485 nm and 490 nm, and excited state absorption (ESA) bands >600 nm. Global fitting of the time evolution of the TA response provided three different kinetic parameters (hence three different time constants) for all three molecules in methanol. In table 2, the global fitting time constants are given. The TA spectra at different time delays along with the fitted kinetics at selected wavelengths for C1, 3Br-C1 and 3I-C1 in methanol are displayed in figures 1a, 1b, 1d, 1e, 1g and 1h, respectively.

The decay associated spectra (DAS) for these three time constants for three molecules are showed in figures 1c, 1f and 1i.

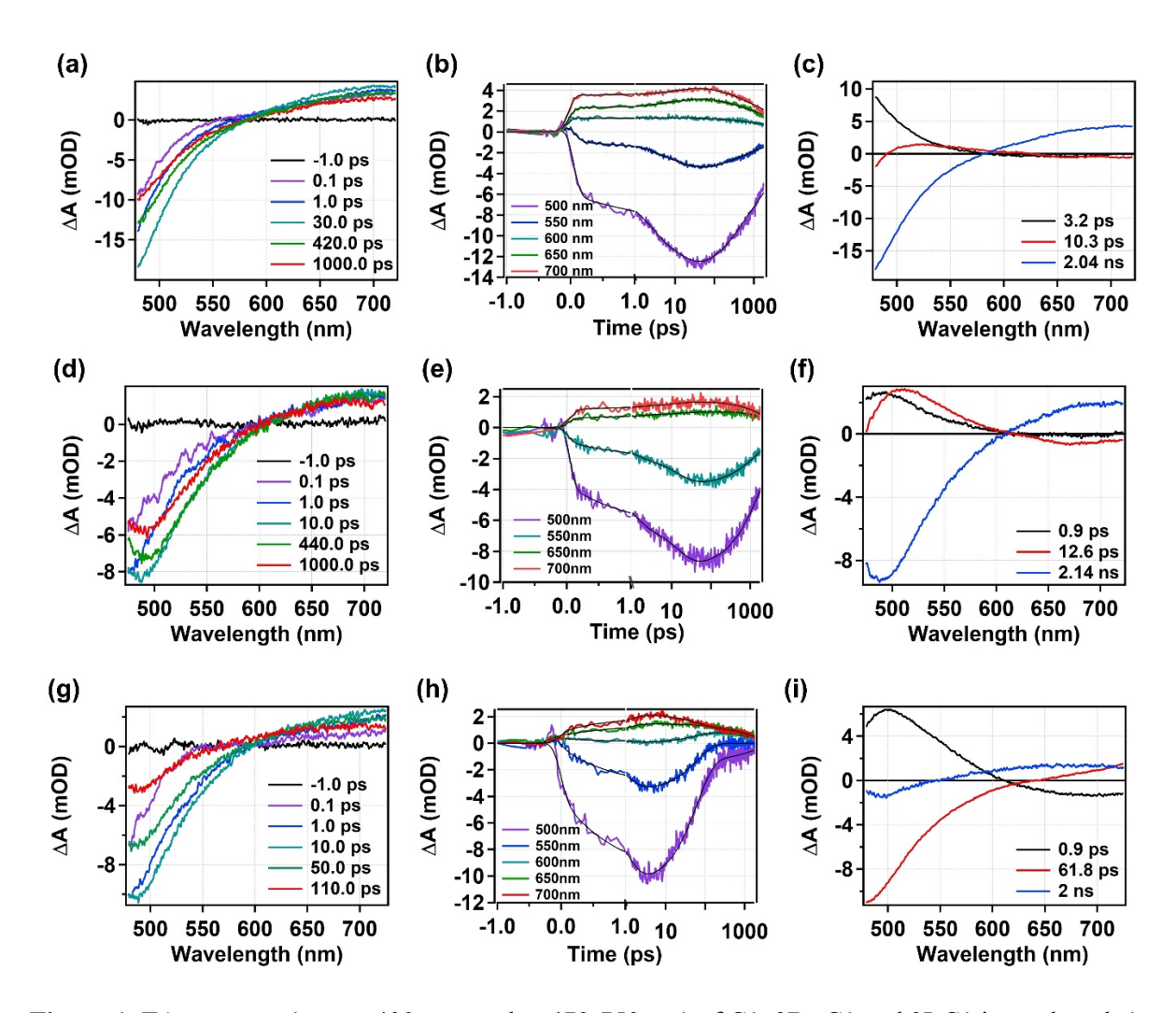


Figure 1. TA response (pump: 400 nm; probe: 470-750 nm) of C1, 3Br-C1 and 3I-C1 in methanol. (a, d, g) TA spectra at some representative delay times for C1, 3Br-C1 and 3I-C1 respectively. For C1, the TA spectra consists of a SE signal around 470 nm and an ESA around 700 nm. For 3Br-C1, The TA spectra consists of a SE signal around 485 nm and an ESA around 700 nm. For 3I-C1, The TA spectra consists of a SE signal around 490 nm and an ESA around 700 nm. (b, e, h) Globally fitted kinetics at some selected wavelengths for C1, 3Br-C1 and 3I-C1 respectively. For C1, obtained time constants from global analysis are 3.2 ps, 10.3 ps and 2.04 ns. For 3Br-C1, obtained time constants from global analysis are 0.9 ps, 12.6 ps and 2.14 ns. For 3I-C1, obtained time constants from global analysis are 0.9 ps, 61.8 ps and 2.0 ns. (c, f, i) Corresponding DAS obtained from global analysis for C1, 3Br-C1 and 3I-C1 respectively.

TD-DFT calculations

All three molecules shown in Scheme 1 were optimized in methanol using PCM model, and their absorption wavelengths were calculated by TD-DFT method. The frontier molecular orbitals of these molecules are displayed in figure S2 and the absorption wavelengths are

tabulated in table S1 along with experimentally obtained absorption wavelengths for comparison. Prompted by previous reports⁴⁴⁻⁴⁹ suggesting rotation of the diethylamino group as a potential deactivation channel for C1, potential energy scan by TDDFT calculation along the diethylamino group rotation coordinate for C1, 3Br-C1 and 3I-C1 was performed. The potential energy curves (PEC) thus obtained for different electronic states are shown in figure S3 of the SI. The PEC along the carbon-halogen bond length was computed, and to our surprise, the PEC for C1, 3Br-C1 and 3I-C1 are observed to be different for the three (figure 2a,b,c). For C1, all the states are bound in nature and there is no crossing of different electronic states. In case of 3I-C1 (figure 2c) S_1 and T_2 state crosses with a slight elongation (~2%) of the C-I bond length. Once the molecule is in T_2 , it is on a downhill trajectory to reach the T_1 surface with 11.3% elongation of the bond length. For 3Br-C1, the crossing between S_1 and S_2 requires 6.1% elongation of the C-Br bond length and eventually reaches the S_2 and S_3 requires 6.1% elongation of the C-Br bond length are eventually reaches the S_4 and S_4 requires 6.1% elongation of the C-Br bond length and eventually reaches the S_4 and S_4 requires 6.1% elongation of the C-Br bond length and eventually reaches the S_4 and S_4 requires 6.1% elongation of the C-Br bond length and eventually reaches the S_4 and S_4 requires 6.1% elongation of the C-Br bond length and eventually reaches the S_4 and S_4 requires 6.1% elongation of the C-Br bond length and eventually reaches the S_4 are crossing, whereas for 3I-C1 the PE barrier is only 0.017 eV.

Given a large atomic SOC constant of Br and I, we further included SOC in the PEC calculation (see figure 2d,e,f for result and Methods section for the details). Though the energy values and the position of surface crossings have changed to some extent, the general features of the SOC-neglected & SOC-incorporated PEC are same. For C1, all the states are bound in nature, as observed without incorporation of SOC (figure 2d). In case of 3I-C1, the crossing between S_1 and T_2 requires a tiniest of bond length modification, and the crossing is almost barrierless (figure 2f). For 3Br-C1, S_1 crosses T_2 after \sim 6 % C-Br bond elongation (figure 2e), with a barrier height of 0.138 eV.

The normal modes of 3I-C1 were computed and it was found that in the ground electronic state 30th & 34th modes lead to change in the carbon-iodine bond length (figure S4 of the SI). The normal modes in the excited electronic states (S₁, T₁ and T₂) at the ground state geometry of 3I-C1 revealed that S₁ normal modes 39 and 46 are in resonance with the T₂ normal modes 42 and 48, respectively. However, T₁ and S₁ are in resonance only through the 39th mode of vibration (figure 3). Most importantly, a close inspection of these normal modes reveals that C-I bond length increases as we move from the S₁ to T₂ manifold through S₁-39:T₂-42 resonating mode (figure 4). The frequency calculations strongly suggest an involvement of bond length variation during ISC, which supports the requirement of the PEC calculations (figure 2) along the varying carbon-halogen bond length.

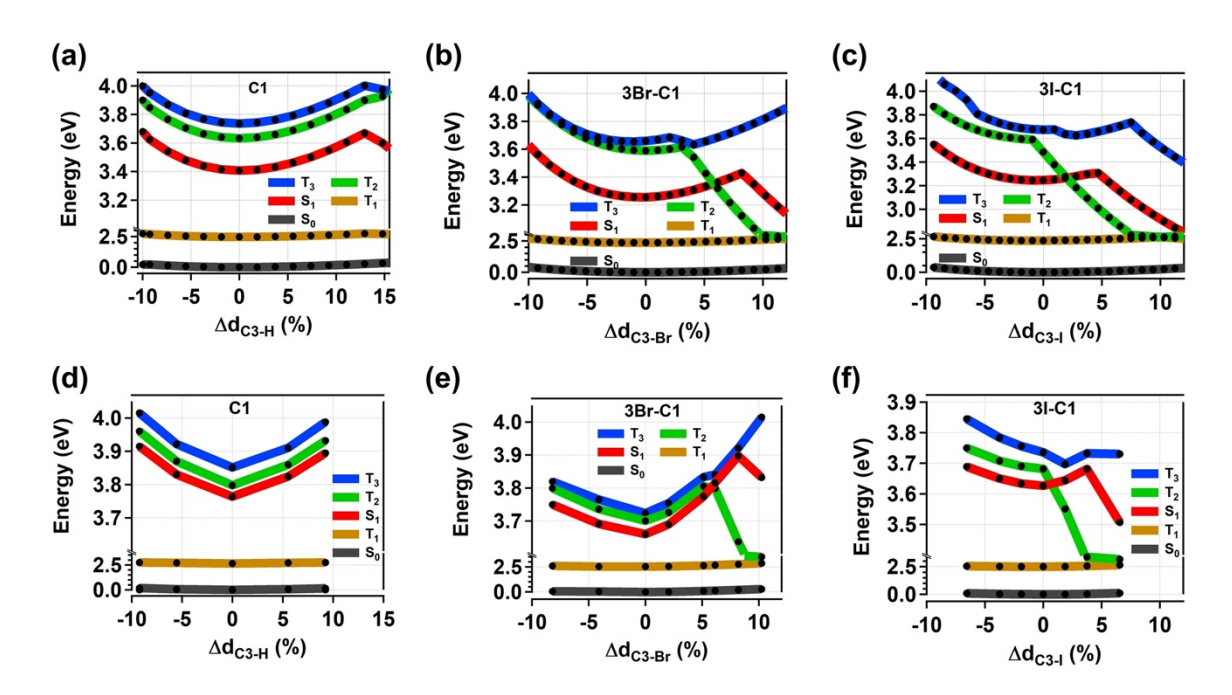


Figure 2. Potential energy curves (PEC) along the C3-X (X=H, Br, I) bond vibration coordinates of the (a) 7-diethylamino-4-methylcoumarin (C1), (b) 3-Bromo-7-diethylamino-4-methylcoumarin (3Br-C1), (c) 3-Iodo-7-diethylamino-4-methylcoumarin (3I-C1) without considering the effect of SOC. SOC-corrected PEC along the C3-X (X=H, Br, I) bond vibration coordinates of the (d) 7-diethylamino-4-methylcoumarin (C1), (e) 3-Bromo-7-diethylamino-4-methylcoumarin (3Br-C1), (f) 3-Iodo-7-diethylamino-4-methylcoumarin (3I-C1). For the PEC calculations without SOC correction, Gaussian 09 package was used. B3LYP exchange correlation functional and 6-311++G (d,p) basis set for C, H, N, O and LANL2DZ basis set for Br and I were used for the TD-DFT calculations to determine the PECs. PE scan was done taking methanol as solvent using PCM model. For the SOC-corrected PEC calculations, B3LYP exchange correlation functional and def2-TZVP basis set was used and calculations are done on Orca 4.2.1 package. $\Delta d_{C3-X}(\%)$ denotes the % change in C3-X (X=H, Br, I) bond length (d_{C3-X}). $\Delta d_{C3-X}(\%) = (\Delta d_{C3-X}(\mathring{A})/d_{C3-X}^{eq}(\mathring{A})) \times 100\%$. d_{C3-X}^{eq} is the equilibrium C3-X bond length in electronic ground state. For molecular structures check scheme 1.

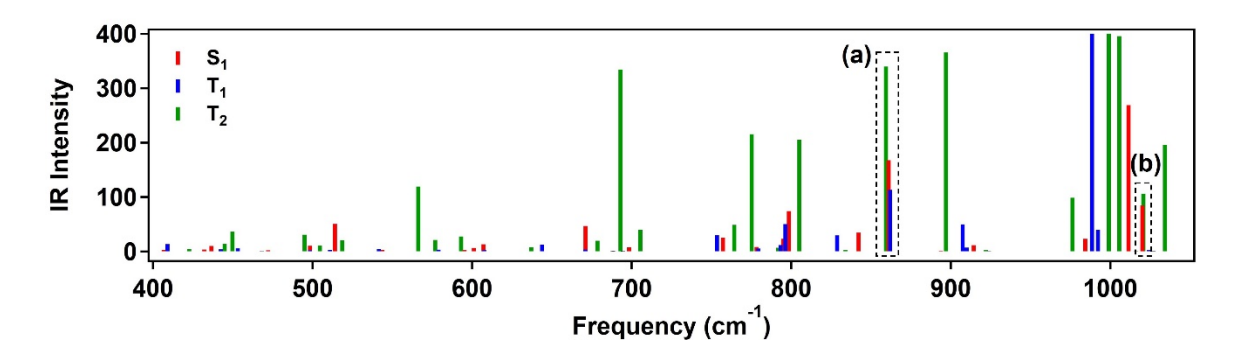
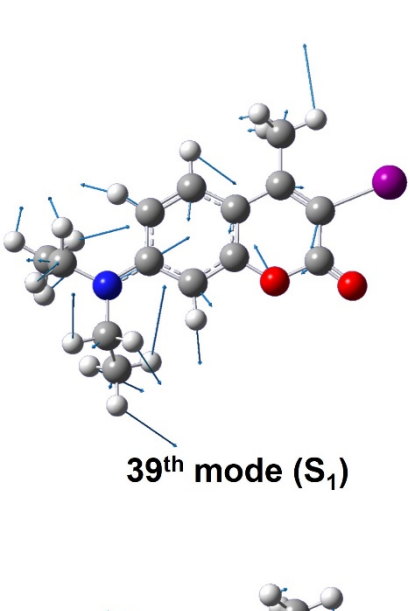


Figure 3. The IR spectra of 3I-C1 in S₁, T₁ & T₂ generated by TD-DFT calculations. The IR signals for normal modes in resonance are squared by dotted line. Square (a) is at 860 cm⁻¹ and square (b) is at 1020 cm⁻¹. Square (a) has the S₁ mode 39, T₁ mode 39 and T₂ mode 42 in resonance and square (b) has the S₁ mode 46 and T₂ mode 48 in resonance. B3LYP exchange correlation functional and 6-311++G (d,p) basis set for C, H, N, O and LANL2DZ basis set for I were used for the frequency calculations.



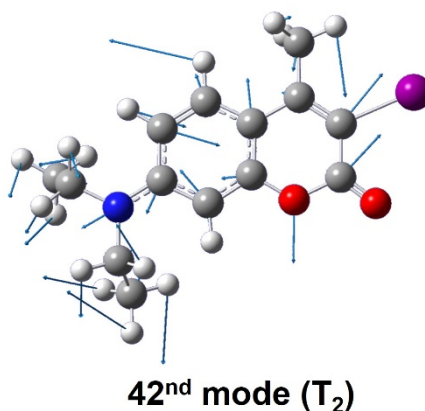


Figure 4. The 39^{th} mode in S_1 and 42^{nd} mode in T_2 of 3I-C1. Blue arrows are indicating displacement vectors. B3LYP exchange correlation functional and 6-311++G (d,p) basis set for C, H, N, O and LANL2DZ basis set for I were used for the frequency calculations. The 39^{th} Mode of S_1 and the 42^{nd} mode of S_2 are resonant (860 cm⁻¹). Close inspection reveals that C-I bond length variation increases as we move from the S_1 to S_2 through these two resonating modes.

Steady state and time-resolved emission studies of octa acid (OA) encapsulated 3-iodo and 3-bromo 7-diethylamino-4-methylcoumarins

Synthetic host octa acid has been established to form closed host-guest capsular complex with C-1 in borate buffer solution. Several guest molecules included within OA capsule are known to phosphoresce at room temperature in solution. To examine the feasibility of phosphorescence from 4-iodo and 4-bromo 7-diethylamino-4-methylcoumarins they were included within OA capsule and emission recorded. NMR study confirmed that all the coumarin derivatives used in this study form a 2:1 (octa acid:coumarin) complex in aqueous buffer medium of pH=7.4 (see figure 5 and section S2 of the SI for details). As seen in figure 5 expected upfield shift of the signals upon complexation is observed (see signals even below δ -1).

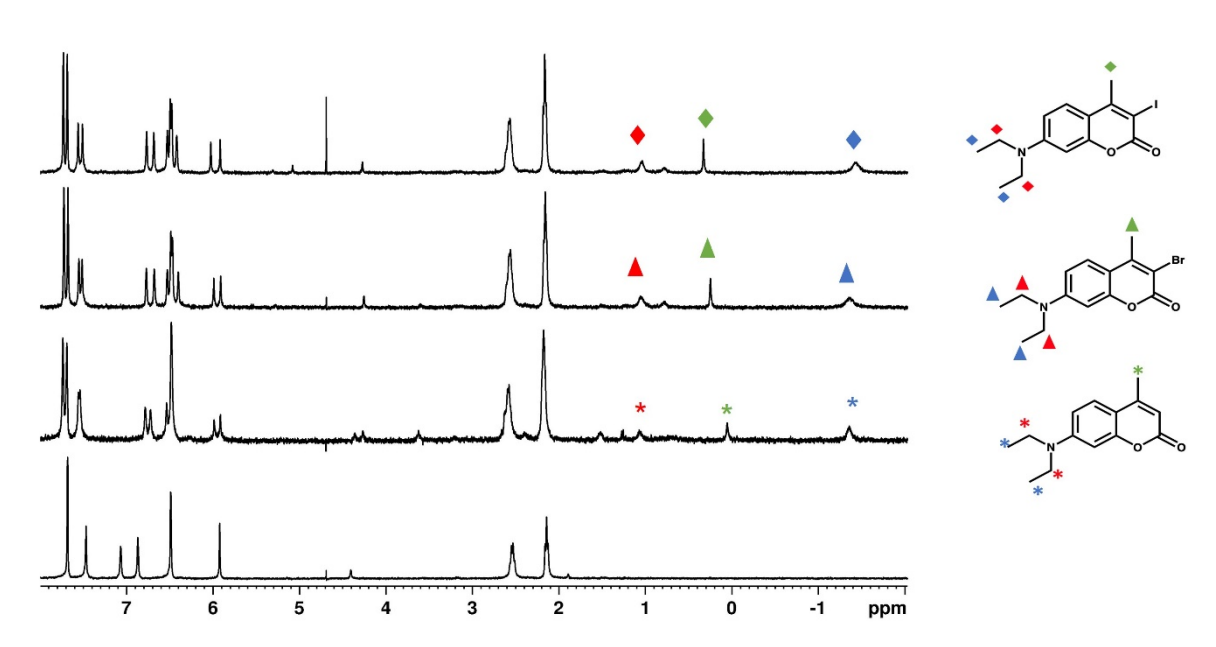


Figure 5. Fig: 1H NMR (400 MHz, 10 mM Na2B4O7 buffer/D2O, pH = 8.7) spectra of (Bottom to top) (i)7-(diethylamino)-4-methyl-2H-chromen-2-one, (ii) 3-bromo-7-(diethylamino)-4-methyl-2H-chromen-2-one in presence of octa acid (OA).

The steady state emission of 3Br-C1@OA₂ and 3I-C1@OA₂ were recorded and are shown in figure 6a. For 3Br-C1@OA₂, a single intense band centered at 440.5 nm is observed. In case of 3I-C1@OA₂, a weak emission band around 580 nm was present along with the intense band centered at 440 nm. With decrease in the temperature, the 580 nm band intensified in the case of 3I-C1@OA₂ (Figure 6b), whereas, for 3Br-C1@OA₂ no change in the emission spectrum is observed. Recorded spectrum of 3I-C1 at 77 K in a glass forming liquid (ethanol-methanol mixture) applying a 500 ns time delay after the excitation showed an intense emission centered at 540 nm confirming the longer wavelength emission to be phosphorescence (see figure 6c). Thus, it is clear that while 3I-C1@OA₂ show phosphorescene at room and low temperature, 3Br-C1@OA₂ does not under both conditions.

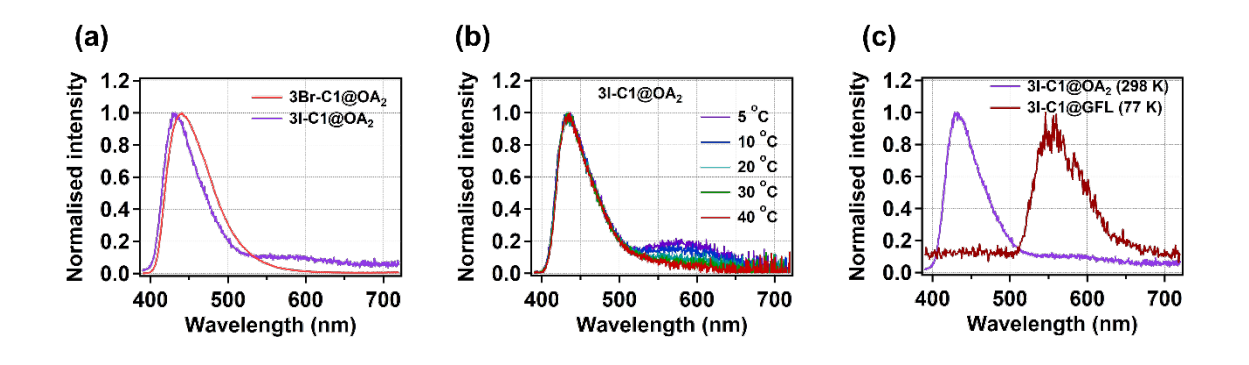


Figure 6. (a) Steady state emission of 3I-C1@OA₂ and 3-Br-C@OA₂ (b) temperature dependence steady state emission of 3I-C1@OA₂ (c) Steady state emission of 3I-C1@OA₂ compared with the phosphorescence spectra of 3I-C1 in glass forming liquid at 77 K. For 3I-C1@OA₂, there is a weak band around 580 nm which is completely absent in case of C1Br@OA₂. This weak emission band for C1I@OA₂ intensifies with decreasing temperature. Phosphorescence spectra recorded for C1I in glass forming liquid (Ethanol-methanol mixture) at 77 K confirms the weak band at 580 nm for C1I@OA₂ as a phosphorescence band.

The TA spectra of 3Br-C1@OA₂ have a strong SE band associated with an ESA band (figure 7). The global fitting analysis of the TA data yielded two time constants of 13.5 ps and 4.6 ns. The TA spectra and the fitted kinetics for some selected time delay and wavelengths and decay associated spectra (DAS) of 3Br-C1@OA₂ are depicted in figure 7a, b, c. On the other hand, the TA spectra for 3I-C1@OA₂ mainly features a broad ESA band, which is stretched throughout the observation window, although in early time a weak SE like feature is observed (figure 7d). The ESA band does not decay in the time delay available in our experimental setup (2 ns). A global fitting analysis yields two time constants, 11.9 ps and >10 ns. In figure 7e we provide fitted kinetics at selected wavelengths and the DAS are shown in figure 7f.

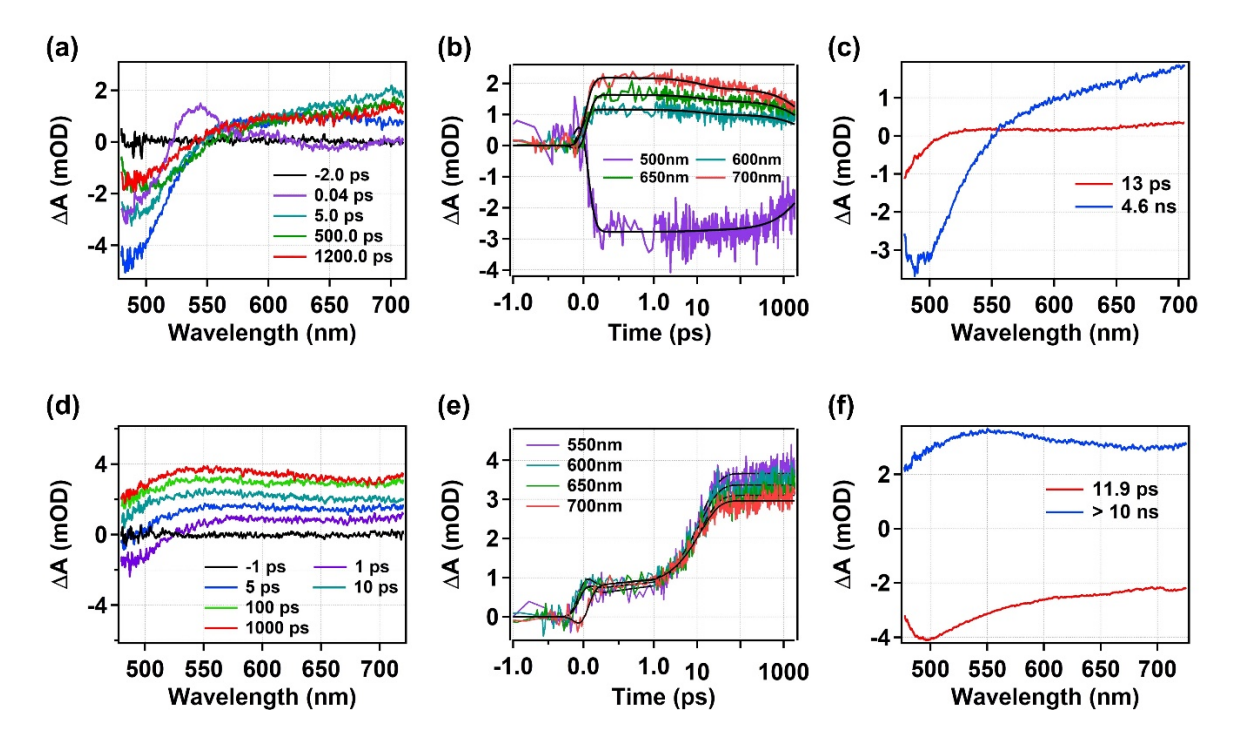


Figure 7. TA response ($\lambda_{ex} = 400 \text{ nm}$; probe: 470-750 nm) of 3Br-C1 and 3I-C1 inside OA cavity. (a, d) TA spectra at some representative delay times for 3Br-C1@OA₂ and 3I-C1@OA₂ respectively. For 3Br-C1@OA₂, the TA spectra consists of a SE signal around 500 nm and an ESA around 600-700 nm. For 3I-C1@OA₂, the TA spectra consists entirely of a broad ESA signal throughout the probe window. (b, e) Globally fitted kinetics at some selected wavelengths for 3Br-C1@OA₂ and 3I-C1@OA₂ and 3I-C

C1@OA₂ respectively. For 3Br-C1@OA₂, obtained time constants from global analysis are 13.0 ps and 4.6 ns. For 3I-C1@OA₂, two time constants were obtained from global analysis. One is of 12 ps and the other is a long time constant \geq 10 ns. (c) Corresponding DAS obtained from global analysis for 3Br-C1@OA₂ and 3I-C1@OA₂ respectively.

Discussion:

From the steady state experiments, in the case of 3I-C1 we observed a decrease in ϕ_f in methanol and cyclohexane, whereas an increase in ϕ_f was observed in case of 3Br-C1 with respect to C1 (Table 1). This observation is not in line with the heavy atom effect, where the ϕ_f is expected to decrease with increasing atomic number of the incorporated halogen. It is known that the introduction of heavy atoms not only promotes the ISC but also facilitates the back intersystem crossing (BISC) process. 51-52 One could attribute the enhanced fluorescence in 3Br-C to BISC. However, presence of BISC for 3Br-C1 but not for the iodo derivative is surprising. Based on the rationale that increasing atomic number should increase both ISC and BISC, one would expect ϕ_f decrease even in the case of 3I-C1.

Explicit analysis of transient absorption data was necessary to understand the photophysics of these coumarins. For C1 in methanol, three time constants from TA analysis were obtained (Table 2). The DAS for 10.3 ps and 2.04 ns components have a prominent SE feature, where the amplitude of the former is smaller compared to the latter (figure 1c). Earlier studies of C1 in polar solvent methanol indicate the operation of a twisted intramolecular charge transfer (TICT) mediated deactivation of the excited state through non-radiative channels. Keeping this in mind, we suspect that the 10.3 ps time component and the associated DAS is of the TICT state of C1 in methanol. The 3.2 ps DAS does not show any SE feature (figure 1c), and we propose this time component is that of the locally excited (LE) state. The SE feature of the 2.04 ns DAS (figure 1c) closely matches with the steady state emission, and hence, we designate it as the solvated TICT state (SS) of C1 in methanol. We attribute the short lifetime of the LE state to rapid shift of the LE population towards the TICT state by twisting and finally to the SS state by solvation.

On the other hand, for 3I-C1, the 0.9 ps DAS looks exactly similar to the short lifetime DAS of C1 and we assign this to the LE state (figure 1i). An SE like feature is observed in both the 61.8 ps and 2.00 ns DAS of 3I-C1. However, unlike in the case of C1, here the 2.0 ns DAS has a low amplitude compared to that of 61.8 ps DAS. The 61.8 ps DAS is the most intense among all and suggests that this state dominates the relaxation process of the excited 3I-C1 leading to a weak fluorescence quantum yield compared to C1. Based on the wavelength of the

SE band, the longest amongst the two, we assign the 2.0 ns DAS to the fully solvated state (SS). However, the weak DAS signal of this state suggests that a very small number of molecules reach this state. We speculate that the decreased intensity is due to the excited 3I-C1 following some other coordinate to reach the triplet state. We cannot confirm the occurrence of ISC solely from this data as we have not seen any DAS associated with this triplet state.

The feature of all three DAS of 3Br-C1 look similar to that of the C1 (figure 1f). Following the assignment in case of C1, we assign the 0.9 ps and 2.14 ns DAS to be associated with the LE and SS sates, respectively. The 12.6 ps DAS of 3Br-C1 is also very similar in feature with that of 10.3 ps DAS of C1, and we assign it to the TICT state of 3Br-C1. Careful examination reveals that the SE feature has been cut off beyond 480 nm due to interference by the probe light. We suspect that though this SE feature is not observed in the measurement window, it is present and can be observed with an extended probe pulse. Unlike 3I-C1, the DAS for SS is the most intense in the case of 3Br-C1. This suggests that the ISC is unfavorable for 3Br-C1, allowing most molecules to reach the SS state.

Earlier reports proposed that the rotation of the diethylamino group of C1 is the predominant coordinate for the formation of the TICT state from the LE state. 45-49 This led us to scan the PE along the rotation of the diethylamino group of the C1, 3Br-C1 and 3I-C1. Examination of figure S3 reveals that the corresponding potential energy curves (PEC) in different electronic states are very similar for the three coumarins. This implies the presence of another coordinate along the PEC that accounts for the variation in ϕ_f . Basically, the studied coumarin derivatives only differ in the substitution at the 3-position of the C1, which hardly affects the twisting of diethylamino group present at the 7-position. This led us to consider a coordinate where the effect of halogen is prominent. There are several reports suggesting how normal mode of vibrations in a molecule can affect ISC as discussed in the introduction section. 12,24 This information prompted us to speculate that the carbon-halogen bond vibration may influence the ISC in the coumarins investigated here. PE scan along this vibrational coordinate showed that the PEC of the electronic states of C1 (in this case there is no halogen substitution, C-X refers to C-H), 3Br-C1 and 3I-C1 are distinctly different for all three (figure 2 in results section). As for C1, all the states are bound in nature, preventing ISC from S₁ (figure 2a). Whereas in case of 3Br-C1 and 3I-C1, crossing between S1 and T2 states are present (figures 2b,c). The S₁-T₂ surface crossing requires much smaller bond deformation for 3I-C1 (~2 %) compared to 3Br-C1 (6.1 %). Most importantly, the PE barrier height for $S_1 \rightarrow T_2$ crossing for 3Br-C1 is significant (0.110 eV) and 6.5 times higher than 3I-C1, which has a PE

barrier of 0.017 eV that is achievable at room temperature. To check the role of SOC on the computed PECs, we have also computed the SOC corrected PECs (Figures 2d,e,f). The nature of the ordering, shapes and intersections of the electronic states remain essentially same. A crossing between S_1 and T_2 was observed in cases of 3Br-C1 and 3I-C1 (figures 2e,f). The higher barrier in 3Br-C1 probably slows the ISC process favoring fluorescence. This could be a possible reason for higher ϕ_f for 3Br-C1 in comparison to 3I-C1. Moreover, excited state frequency calculation for 3I-C1 suggests that certain modes of vibration in S_1 and T_2 are in resonance with each other (figure 3) but the C-I bond length change is much more prominent in case of T_2 compared to S_1 (figure 4). Thus, S_1 to T_2 jump must involve the C-I bond length variation coordinate.

The TA analysis along with TD-DFT calculations have provided a glimpse of the photophysics associated with halogen derivatives of C1. However, the association of state mixing and solvation process have made the problem somewhat difficult to address. The poor stability of triplets due to oxygen quenching makes the experimental measurements slightly difficult.⁵³ It has been established earlier that one could protect the phosphorescent molecules by including it within an organic capsule formed from octa acid (OA) host. 54-55 The internal OA cavity of OA capsule is established to be non-polar in nature. ⁵⁶⁻⁵⁷ Consistent with the nonpolar character and the tightness of the cavity no solvation of the excited coumarin occurred within the OA cavity.⁵⁸ It is also known that molecular oxygen do not penetrate the OA cavity.⁵⁹ Most importantly, the small OA cavity with very little free space will not allow the large amplitude motion of the diethylamino group twisting and the TICT state will not be expected. Thus, we can anticipate phosphorescence from OA encapsulated 3I-C1 and 3Br-C1 if any triplet state is involved in the excited state deactivation of these molecules. In case of 3I-C1@OA₂, the presence of a broad band emission at longer wavelength (580 nm) along with the usual fluorescence (440 nm) and its gradual increase with lowering of temperature (figure 6) confirm the long wavelength emission to be phosphorescence from the triplet. Timedelayed low temperature emission (77 K) of 3I-C1 in the glass forming liquid (ethanolmethanol mixture) shows an emission band around 540 nm. This also supported that the longer wavelength temperature dependent weak broadband emission observed for 3I-C1 inside OA cavity is room temperature phosphorescence.

In the transient absorption signal of 3I-C1@OA₂, the broad ESA band along with the long lifetime component clearly indicates the existence of the triplet state in case of 3I-C1@OA₂ (figure 7). Usually, the triplet states are closely spaced in terms of electronic energy

and thus it is not surprising that the ESA band for a triplet state being broad in nature. We assign the >10 ns component as the triplet state and the 11.9 ps component to the S_1 state of $3I-C1@OA_2$ the precursor for the triplet state. Based on the above observations, we propose that in $3I-C1@OA_2$ it is the C-I vibration that takes the system to the T_1 state. We believe that due to this bond vibration mediated channel the S_1 state has a very short lifetime of 11.9 ps.

For 3Br-C1@OA₂, the 4.6 ns DAS has a strong SE feature (figure 7c), and we assign it to the lifetime of the S₁ state of 3Br-C1@OA₂. The short lifetime (13.5 ps) DAS mostly consists of an ESA band with a SE band at the blue edge of the observation window (figure 7c). We suspect this short lifetime component is associated with another emissive state, which resides on a completely different nuclear coordinate on the PES. At this stage we have no knowledge of its structure.

The above theoretical and experimental studies suggest that the C–X (X=Br/I) bond vibration coordinate plays an important role on the fate of the excited singlet state of 3Br-C1 and 3I-C1. This also rationalizes the unusually high ϕ_f of 3Br-C1 compared to 3I-C1. However, the higher ϕ_f of 3Br-C1 compared to the parent C1, cannot be explained either by the C–X vibration or by the diethylamino twisting coordinates. We consider two reasons for this unusual behavior. First, we believe the reason lies on a different reaction coordinate, namely the solvent polarization coordinate. From the previous works we know that for similar coumarins like C1, there is an extra relaxation path from TICT \rightarrow ground state via solvent fluctuation. The nonradiative transition from the TICT to the GS happens to be PE barrier mediated. The difference in this barrier height for C1 and 3Br-C1 is a plausible reason behind the higher ϕ_f of 3Br-C1 compared to C1. Secondly, from earlier reports it is evident that fluorescence quantum yield (ϕ_f) is related with the π -conjugation length (A_π) . Longer the conjugation more efficient is the fluorescence. Lamber of the shown that, the ϕ_f is related to the A_π as (see SI for derivation) $^{61-62}$

$$\phi_f = \frac{1}{\frac{c^3}{8\pi h v^3} e^{-A_{\pi+1}}} \tag{1}$$

The parameter A_{π} can be think of as the change in dipole moment ($\Delta \mu = \mu_e - \mu_g$) upon photoexcitation. ⁶¹⁻⁶² From Lippert-Mataga formulation we can write

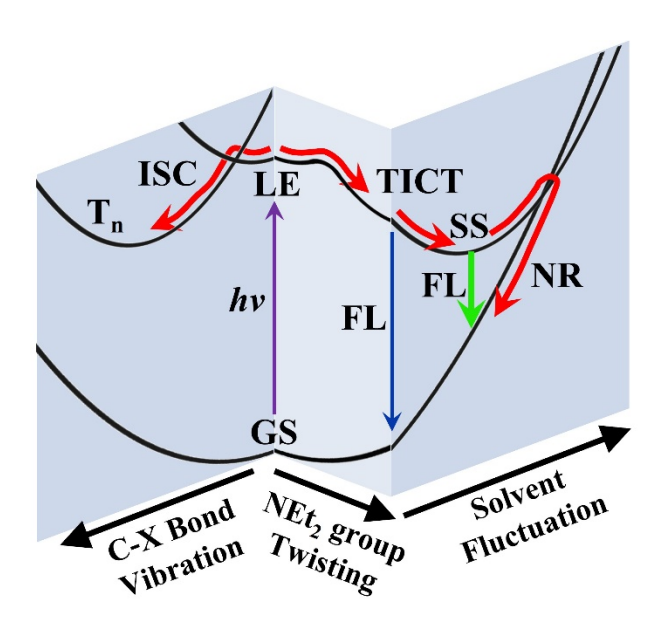
$$\Delta\mu \propto \left(\bar{\nu}_a - \bar{\nu}_f\right)^{1/2} a^{3/2} \tag{2}$$

Hence, equation 1 reforms into

$$\phi_f = \frac{1}{\frac{c^3}{8\pi\hbar^{3}}e^{-(\bar{\nu}_a - \bar{\nu}_f)^{1/2}a^{3/2} + 1}}$$
(3)

Where \bar{v}_a is the wavenumber of absorption and \bar{v}_f is the wavenumber of fluorescence, which are known from the steady state data. The a is the molecular radii and was determined from the DFT calculations. Using all these inputs, we find that the $\Delta\mu$ trend for the three coumarins are 3Br-C1 \approx 3I-C1>C1. Therefore, the ϕ_f order should also be 3Br-C1 \approx 3I-C1>C1.

This estimated ϕ_f order will only be valid for a set of molecules for which there is no extra non-radiative deactivation channel operational for any one of them. In case of 3I-C1, the ISC channel is extremely favourable, which decreases the actual ϕ_f of 3I-C1 from the value estimated by equation 3. On the other hand, as in case of both C1 and 3Br-C1, ISC is unfavourable, the estimated ϕ_f order between them holds in reality. This explains the higher ϕ_f of 3Br-C1 compared to C1.



Scheme 2. A general relaxation scheme for photo-excited 3X-C1 (X= H, Br, I). Depending upon X and medium, the PE barrier on each coordinate varies. Thus, for a particular molecule in a particular medium relaxation through some coordinate becomes predominant whereas relaxation through the other paths become negligible.

We present a scheme for the overall relaxation processes of photoexcited 3X-C1 (X= H, Br, I) in scheme 2. Following excitation, they can follow the diethylamino twisting coordinate to reach the TICT state followed by solvation of the TICT to SS. At the same time, the system can also reach the triplet state through a different co-ordinate namely carbonhalogen bond vibration. The propensity of ISC path along the vibration coordinate depends on the barrier height present along the bond vibration coordinate. According to the results presented above, the preferred relaxation channel depends strongly on the nature and position

of halogen substitution. For example, as the barrier height between the singlet (S_1) and triplet (T_2) states along the bond vibration coordinate is negligible for 3I-C1 (see figure 2c), it prefers to follow this path rather than the one which leads to SS. It explains the lack of fluorescence in 3I-C1. On the other hand, in 3Br-C1 the barrier height between the same singlet and triplet states along the C-Br vibration coordinate is significant (see figure 2b). Most likely this forces the molecule to avoid this path relative to TICT pathway leading to SS. Similar is the case for C1. In this case there is no crossing between singlet and triplet surfaces and therefore it reaches the SS via the only available diethylamino twisting coordinate (see figure 2a). In scheme 2, only the relaxation of the most stable form of the TICT along the solvent fluctuation coordinate is shown. Due to solvent fluctuation, the SS state crosses with the GS through an energy barrier at a particular solvent orientation where the solvated TICT (i.e. SS) and GS are isoenergetic. ⁶⁰ We propose that the difference in this barrier height is a plausible explanation of higher ϕ_f value for 3Br-C1 than C1. The scheme 2 will depend on the medium. For example, inside OA capsule the solvent fluctuation coordinate will be insignificant as the capsule interior lacks any solvent. ⁵⁸

To examine whether the involvement of C–X bond vibration in ISC is a general feature, a similar approach was taken to a completely different yet simpler molecular system, namely 1-iodonaphthalene, 1-bromonaphthalene and 2-bromonaphthalene (1I-Nap, 1Br-Nap, and 2Br-Nap, respectively). The ratio of the square of SOC constant to ISC rate constants for 1I-Nap and 1Br-Nap-are 0.5 and 1.1, respectively. 10,12 The PECs along the C–X bond length coordinate of all the three molecules were constructed by TD-DFT calculation (see figure 8). For 1I-Nap a crossing between S₁ and T₄ states has been noticed around the LE state, and its difference compared to the Br-counterparts are distinctly visible. On the other hand, both 1Br-Nap and 2Br-Nap must undergo bond elongation before reaching the crossing point between S₁ and T₅. The difference in the PE barrier to the triplet crossing for 1Br-Nap and 2Br-Nap is evident, where it is smaller in the former. The experimental observation of ϕ_f of 1Br-Nap (0.67%) and 2Br-Nap (1.25%) are proposed to be due to the difference in PE barrier along the C-Br bond vibration coordinate. However, for a precise comment on this, higher level theoretical calculations are necessary. This agreement between theoretical prediction and experimental result indicates that this model based on molecular vibrations should be useful for future studies on the effect of position dependent substitution on the ISC rate.

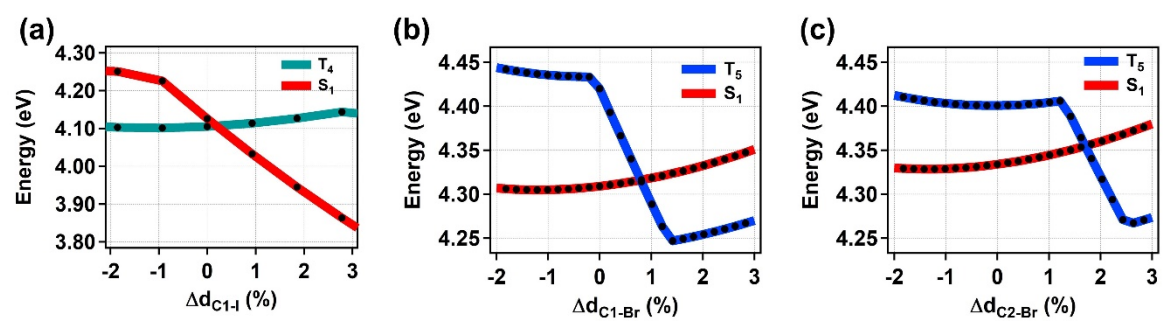


Figure 8. Potential energy curves (PEC) along the Cn-X (n=1, 2; X=Br, I) bond vibration coordinate for the (a) 1-Iodo-naphthalene (1I-Nap), (b) 1-Bromo-naphthalene (1Br-Nap) and (c) 2-Bromo-naphthalene (2Br-Nap). For better clarity only the S₁ and T₄ surfaces for 1I-Nap and the S₁ and T₅ surfaces for 1Br-Nap and 2Br-Nap were plotted. B3LYP exchange correlation functional and 6-311++G (d,p) basis set for C & H and LANL2DZ basis set for Br and I were used for the TD-DFT calculations to determine the PECs. $\Delta d_{Cn-X}(\%)$ denotes the % change in Cn-X (n=1, 2; X=Br, I) bond length (d_{Cn-X}) . $\Delta d_{Cn-X}(\%) = (\Delta d_{Cn-X}(\mathring{A})/d_{Cn-X}^{eq}(\mathring{A})) \times 100\%$. d_{Cn-X}^{eq} is the equilibrium Cn-X bond length in electronic ground state.

We also use this approach to predict the trend of ISC and ϕ_f for the other possible halosubstituted coumarin 1 derivatives, namely 5-bromo-coumarin 1 (5Br-C1), 6-bromo-coumarin 1 (6Br-C1), 8-bromo-coumarin 1 (8Br-C1), 5-iodo-coumarin 1 (5I-C1), 6-iodo-coumarin 1 (6I-C1) and 8-iodo-coumarin 1 (8I-C1). The structures of these molecules are given in scheme S3 of the SI. The PECs along the C-halogen bond length for these halo-derivatives are displayed in figure S7 of the SI. For all these molecules crossing of S₁ and T₃ states can be found at some point of the C-X(X=Br/I) bond length variation coordinate. At this level of theory, a precise prediction of the values of PE barrier is not possible. However, it is obvious that the barrier height to reach the S₁-T₃ crossing is different for all these molecules that depends on the position of the Br/I substitution. We expect the fluorescence quantum yields to increase or decrease as the PE barriers decrease or increase. To check the validity of the above results, synthesis of these molecules and the subsequent determination of their fluorescence quantum yield is necessary, which is reserved for the future.

Present study suggests that for the molecular systems where a strong coupling between states is present along the vibrational coordinates, Marcus theory is valid and rate constant of ISC and free energy barrier should be correlated. We believe that with proper choice of a molecular system one can experimentally verify this prediction. We plan to pursue this line of of approach in the near future.

Conclusions:

Iodo substitution of the parent coumarin C1 decreases the fluorescence quantum yield to a large extent as expected, whereas the bromo substitution of C1 surprisingly increases the fluorescence quantum yield. This anomalous observation could not be understood from the viewpoint of conventional SOC constants alone. Detailed TA experiments and TD-DFT calculations reveal that C-X bond vibration controls the ISC in these halo-coumarins and hence dictates the whole excited state relaxation process of 3Br-C1 and 3I-C1. The time constant of ISC for 3I-C1 is 11.9 ps, whereas it is forbidden in case of 3Br-C1. Presence of 0.12 eV PE barrier on the C3-Br bond vibration coordinate is thought to be responsible for the slow ISC in the case of 3Br-C1. Vibration controlled ISC was also observed for halo-naphthalenes, where SOC approach fails to fully predict the extent of ISC, but the model based on bond vibration does. We also have successfully predicted the position dependency of halogen insertion on fluorescence quantum yield using the model. Overall, we propose that C-X bond vibration plays a crucial role in ISC. It also explains the effect of heavy atom insertion in different position of a molecule. We believe that while engineering RTP molecules using heavy atom, one should always consider the position dependence of heavy atom insertion. PES constructed using TD-DFT calculations for the targeted molecules, is likely to reveal the position in which halogen insertion will give most efficient ISC. We are optimistic that Marcus inversion in ISC will be observed in the future by examining a series of molecules chosen based the C-X vibrational model discussed here. To achieve this goal extensive experimental, theoretical and synthetic studies are required.

ASSOCIATED CONTENT

Supporting Information: Synthesis procedure of 3Br-C1 & 3I-C1, steady state absorption and emission spectra of C1, 3Br-C1 & 3I-C1 in cyclohexane & methanol, PEC of the coumarins along the -NEt₂ group rotation, normal modes of vibration for 3I-C1 in its ground electronic state, NMR data for the coumarin-OA complexation, molecular structures and PEC along carbon-halogen bond vibration of some other bromo/iodo-derivatives of C1 and derivation of relation between the fluorescence quantum yield (ϕ_f) and the π -conjugation length (A_{π}) are included in the supporting information.

AUTHOR INFORMATION

Aritra Das – Department of Chemistry, Indian Institute of Technology Kanpur, Kanpur – 208 016, UP, India; orcid.org/0000-0002-8251-8190; Email: aritrad@iitk.ac.in

Sujit Kumar Ghosh – Department of Chemistry, University of Miami, Coral Gables, Florida 33146, United States; orcid.org/0000-0003-3849-5996; Email: sxg1339@miami.edu V. Ramamurthy – Department of Chemistry, University of Miami, Coral Gables, Florida 33146, United States; orcid.org/0000-0002-3168-2185; Email: murthy1@miami.edu Pratik Sen – Department of Chemistry, Indian Institute of Technology Kanpur, Kanpur – 208 016, UP, India; orcid.org/0000-0002-8202-1854; Email: psen@iitk.ac.in

ACKNOWLEDGMENTS

A.D. acknowledges Ministry of Electronics & Information Technology (MeitY), Government of India for providing fellowship under the Visvesvaraya PhD scheme. V.R. thanks the National Science Foundation (CHE-1807729) for financial support. P.S. thanks Indian Institute of Technology Kanpur for infrastructure. We acknowledge Ms. Kanyashree Jana and Prof. J. N. Moorthy of Indian Institute of Technology Kanpur for low-temperature emission measurement. We thank Dr. Sougata Pal of Department of Chemistry, University of Gour Banga, India for useful discussion on incorporation of SOC in quantum chemical calculation.

References

- Jena, S.; Dhanalakshmi, P.; Bano, G.; Thilagar, P. Delayed Fluorescence, Room Temperature Phosphorescence, and Mechanofluorochromic Naphthalimides: Differential Imaging of Normoxia and Hypoxia Live Cancer Cells. *J. Phys. Chem. B* 2020, *124*, 5393-5406.
- 2. Kuila, S.; Garain, S.; Banappanavar, G.; Garain, B. C.; Kabra, D.; Pati, S. K.; George, S. J. Ambient Room Temperature Phosphorescence and Thermally Activated Delayed Fluorescence from a Core-Substituted Pyromellitic Diimide Derivative. *J. Phys. Chem. B* **2021**, *125*, 4520-4526.
- 3. Hirata, S.; Bhattacharjee, I. Vibrational Radiationless Transition from Triplet States of Chromophores at Room Temperature. *J. Phys. Chem. A* **2021**, *125*, 885-894.
- 4. Lai, L.; Fang, B.; Fan, M.; Cheng, W.; Yin, M. Modulating Room-Temperature Phosphorescence through the Synergistic Effect of Heavy-Atom Effect and Halogen Bonding. *J. Phys. Chem. C* **2021**, *125*, 16350-16357.
- 5. Grotjahn, R.; Kaupp, M. Reliable TDDFT Protocol Based on a Local Hybrid Functional for the Prediction of Vibronic Phosphorescence Spectra Applied to Tris(2,2'-bipyridine)-Metal Complexes. *J. Phys. Chem. A* **2021**, *125*, 7099-7110.
- 6. Kasha, M. The triplet state: An example of G. N. Lewis' research style. *J. Chem. Edu.* **1984**, *61*, 204-215.
- 7. Lewis, G. N., Kasha, M. Phosphorescence and the Triplet State. *J. Am. Chem. Soc.* **1944**, 66, 2100–2116.
- 8. Lewis, G. N., Kasha, M. Phosphorescence in Fluid Media and the Reverse Process of Singlet-Triplet Absorption. *J. Am. Chem. Soc.* **1945**, *67*, 994–1003.
- 9. Kasha, M. Phosphorescence and the Role of the Triplet State in the Electronic Excitation of Complex Molecules. *Chem. Rev.* **1947**, *41*, 401–419.
- 10. McClure, D. S. Triplet-Singlet Transitions in Organic Molecules. Lifetime Measurements of the Triplet State. *J. Chem. Phys.* **1949**, *17*, 905-913.
- 11. Turro, N. J.; Ramamurthy, V.; Scaiano, J. C. Modern Molecular Photochemistry of Organic Molecules; University Science Books: Sausalito, CA, 2010. pp 249-257.
- 12. Solovyov, K. N.; Borisevich, E. A. Intramolecular Heavy-Atom Effect in the Photophysics of Organic Molecules. *Phys.-Usp.* **2005**, *48*, 231–253.
- 13. El-Sayed, M. A Theoretical Considerations Concerning the Intramolecular Heavy-Atom Effect on the Phosphorescence Process: C_{2v} Symmetric Dihalonaphthalene *J. Chem. Phys.* **1965**, *43*, 2864-2872.

- 14. Murata, S.; Iwanaga, C.; Toda, T.; Kokubun, H. Fluorescence and radiationless transitions from the second excited states of azulene derivatives *Ber. Bunseges. Phys. Chem.* **1972**, *76*, 1176-1183.
- 15. Eber, G.; Schneider, S.; Dorr, F. On the importance of intersystem crossing for the deactivation of the S2 state of halogeno derivatives of azulene. *Chem. Phys. Lett.* **1977**, *52*, 59-62.
- Abou-Zied, O. K.; Sinha, H. K.; Steer, R. P. Van der Waals Complexes of 2-Chloro-, 2-Methyl-, and 1,3-Dimethylazulene with Rare Gases: Microscopic Solvent Shifts,
 Structures, and Binding Energies. *J. Phys. Chem. A* 1997, 101, 7989-7997.
- 17. Roy, J. K.; Goodman, L. Halogen enhancement of singlet-triplet transitions: Part I. Low-resolution polarization of halophenanthrene spectra. *J. Mol. Spectrosc.* **1966**, *19*, 389-406.
- 18. Ginsburg, J. L.; Goodman, L. Halogen Enhancement of Singlet–Triplet Transitions. II. Vibronic Paths in Phenanthrene. *J. Chem. Phys.* **1970**, *52*, 2369-2374.
- 19. Najbar, J.; Jarzeba, W.; Urbanek, Z. H. Internal heavy-atom effect on the T1 states of monochloroquinolines and monochloronaphthalenes. *Chem. Phys.* **1983**, *79*, 245-253.
- 20. Najbar, J.; Jarzeba, W.; Hochstrasser, R. M. Non-radiative decay of the T1 states of chloronaphthalenes and protonated chloroquinolines at 77 K. *Chem. Phys.* **1985**, *95*, 1-8.
- 21. Jarzeba, W.; Najbar, J.; Cioslowski, J. Internal heavy atom effects for chloro- and bromoquinolines. *J. Mol. Struct.* **1986**, *141*, 469-474.
- 22. Lewanowicz, A.; Lipinski, J.; Ruziewicz, Z.; Szymczak, A.; Szynkarczuk, J. Position-dependent effects of internal heavy atoms on highly resolved electronic spectra and luminescence properties of some quinoxalines substituted at the homocyclic ring. *J. Lumin.* **1989**, *43*, 85-102.
- 23. El-Sayed, M. Spin Orbit Coupling and the Radiation-less Processes in Nitrogen Heterocyclics. *J. Chem. Phys.* **1963**, *38*, 2834–2838.
- 24. Thomas J. Penfold, T. J.; Gindensperger, E.; Daniel, C; Marian, C. M. Spin-Vibronic Mechanism for Intersystem Crossing. *Chem. Rev.* **2018**, *118*, 6975–7025.
- 25. Turro, N. J.; Ramamurthy, V.; Scaiano, J. C. Principles of Molecular Photochemistry: An Introduction; University Science Books: Mill Valley, CA, 2015. p 133.
- 26. Englman, R.; Jortner, J. The Energy Gap Law for Radiationless Transitions in Large Molecules. *Mol. Phys.* **1970**, *18*, 145–164.
- 27. Etinski, M.; Marian, C. M. Overruling the Energy Gap Law: Fast Triplet Formation in 6-azauracil. *Phys. Chem. Chem. Phys.* **2010**, *12*, 15665–15671.

- 28. Lemke, H. T.; Kjær, K. S.; Hartsock, R.; Van Driel, T. B.; Chollet, M.; Glownia, J. M.; Song, S.; Zhu, D.; Pace, E.; Matar, S. F.; et al. Coherent Structural Trapping Through Wavepacket Dispersion During Photoinduced Spin State Switching. *Nat. Commun.* **2017**, *8*, 15342.
- Cannizzo, A.; Blanco-Rodríguez, A. M.; El Nahhas, A.; Ebera, J. S.; Zalis, S.; Vlcek, A. J.; Chergui, M. Femtosecond Fluorescence and Intersystem Crossing in Rhenium(I)
 Carbonyl-Bipyridine Complexes. J. Am. Chem. Soc. 2008, 130, 8967–8974.
- 30. van der Veen, R. M.; Cannizzo, A.; van Mourik, F.; Vlcek, A. J.; Chergui, M. Vibrational Relaxation and Intersystem Crossing of Binuclear Metal Complexes in Solution. *J. Am. Chem. Soc.* **2011**, *133*, 305–315.
- 31. Mondal, P.; Opalka, D.; Poluyanov, L. V.; Domcke, W. Jahn- Teller and Spin-Orbit Coupling Effects in Transition-Metal Trifluorides. *Chem. Phys.* **2011**, *387*, 56–65.
- 32. Parker, D.; Minns, R.; Penfold, T.; Worth, G.; Fielding, H. Ultrafast Dynamics of the S1 Excited State of Benzene. *Chem. Phys. Lett.* **2009**, *469*, 43–47.
- 33. Minns, R. S.; Parker, D. S. N.; Penfold, T. J.; Worth, G. A.; Fielding, H. H. Competing Ultrafast Intersystem Crossing and Internal Conversion in the "Channel 3" Region of Benzene. *Phys. Chem. Chem. Phys.* **2010**, *12*, 15607–15615.
- 34. Penfold, T.; Spesyvtsev, R.; Kirkby, O. M.; Minns, R.; Parker, D.; Fielding, H.; Worth, G. Quantum Dynamics Study of the Competing Ultrafast Intersystem Crossing and Internal Conversion in the "channel 3" Region of Benzene. *J. Chem. Phys.* **2012**, *137*, 204310.
- 35. Marian, C. M. On the Mechanism of the Triplet-to-Singlet Upconversion in the Assistant Dopant ACRXTN. *J. Phys. Chem. C* **2016**, *120*, 3715–3721.
- 36. Gibb, C. L. D.; Gibb, B. C. Well-defined, organic nanoenvironments in water: The hydrophobic effect drives a capsular assembly. *J. Am. Chem. Soc.* **2004**, *126*, 11408-11409.
- 37. Kitamura, K.; Ieda, N.; Hishikawa, K.; Suzuki, T.; Miyata, N.; Fukuhara, K.; Nakagawa, H. Visible light-induced nitric oxide release from a novel nitrobenzene derivative cross-conjugated with a coumarin fluorophore. *Bioorg. Med. Chem. Lett.* **2014**, *24*, 5660-5662.
- 38. Wirtz, L.; Kazmaier, U. A Mild Titanium-Catalyzed Synthesis of Functionalized Amino Coumarins as Fluorescence Labels. *Eur. J. Org. Chem.* **2011**, *35*, 7062-7065.
- 39. Mukherjee, P.; Das, A.; Sengupta, A.; Sen, P. Bimolecular Photoinduced Electron Transfer in Static Quenching Regime: Illustration of Marcus Inversion in Micelle. *J. Phys. Chem. B* **2017**, *121*, 1610–1622.

- 40. Das, A.; Kamatham, N.; Mohan Raj, A.; Sen, P.; Ramamurthy, V. Marcus Relationship Maintained During Ultrafast Electron Transfer Across a Supramolecular Capsular Wall. *J. Phys. Chem. A* **2020**, *124*, 5297–5305.
- 41. Das, A.; Danao, A.; Banerjee, S.; Mohan Raj, A.; Sharma, G.; Prabhakar, R.; Srinivasan, V.; Ramamurthy, V.; Sen, P. Dynamics of Anthracene Excimer Formation within a Water-Soluble Nanocavity at Room Temperature. *J. Am. Chem. Soc.* **2021**, *143*, 2025–2036.
- 42. Frisch, M. J.; Trucks, G. W.; Schlegel, H. B.; Scuseria, G. E.; Robb, M. A.; Cheeseman, J. R.; Scalmani, G.; Barone, V.; Petersson, G. A.; Nakatsuji, H.; et al. Gaussian 09, Rev. D01; Gaussian, Inc.: Wallingford, CT, 2016
- 43. Neese, F.; Wennmohs, F.; Becker, U.; Riplinger, C. The ORCA Quantum Chemistry Program Package. *J. Chem. Phys.* **2020**, *152*, 224108.
- 44. Jones, G.; Jackson, W. R.; Choi, C. Y.; Bergmark, W. R. Solvent Effects on Emission Yield and Lifetime for Coumarin Laser Dyes. Requirements for a Rotatory Decay Mechanism. *J. Phys. Chem. C* **1985**, *89*, 294–300.
- 45. Barik, A.; Kumbhakar, M.; Nath, S.; Pal, H. Evidence for the TICT mediated nonradiative deexcitation process for the excited coumarin-1 dye in high polarity protic solvents, *Chem. Phys.* **2005**, *315*, 277–285.
- 46. Arbeloa, T. L.; Arbeloa, F. L.; Estevez, M. J. T.; Arbeloa, I. L. Binary solvent effects on the absorption and emission of 7-aminocoumarins. *J. Lumin.* **1994**, *59*, 369-375.
- 47. Ramalingam, A.; Sivaram, B.M.; Palanisamy, P. K.; Masilamani, V. Photophysics of TICT states of 7-diethylamino-4-methyl coumarin dye by energy transfer techniques. *Spectrochim. Acta Part A* **2000**, *56*, 1205–1210.
- 48. Barik, A.; Nath, S.; Pal, H. Effect of solvent polarity on the photophysical properties of coumarin-1 dye. *J. Chem. Phys.* **2003**, *119*, 10202.
- 49. Barik, A.; Kumbhakar, M.; Nath, S.; Pal, H. Evidence for the TICT mediated nonradiative deexcitation process for the excited coumarin-1 dye in high polarity protic solvents. *Chem. Phys.* **2005**, *315*, 277–285.
- 50. Ramamurthy, V. Photochemistry within a Water-Soluble Organic Capsule. *Acc. Chem. Res.* **2015**, *48*, 2904–2917.
- 51. Drummond, B. H.; Hoover, G. C.; Gillett, A. J.; Aizawa, N.; Myers, W. K.; McAllister, B. T.; Jones, S. T. E.; Pu, Y.-J.; Credgington, D.; Seferos, D. S. Selenium Substitution Enhances Reverse Intersystem Crossing in a Delayed Fluorescence Emitter. *J. Phys. Chem. C* 2020, *124*, 6364-6370.

- 52. Aizawa, N.; Harabuchi, Y.; Maeda, S.; Pu, T.-J. Kinetic prediction of reverse intersystem crossing in organic donor–acceptor molecules *Nat. Commun.* **2020**, *11*, 3909
- 53. Grewer, C.; Brauer, H. D. Mechanism of the Triplet-State Quenching by Molecular Oxygen in Solution. *J. Phys. Chem.* **1994**, *98*, 4230–4235
- 54. Jayaraj, N.; Maddipatla, M. V. S. N.; Prabhakar, R.; Jockusch, S.; Turro, N. J.; Ramamurthy, V. Closed Nanocontainer Enables Thioketones to Phosphoresce at Room Temperature in Aqueous Solution. *J. Phys. Chem. B* **2010**, *114*, 14320–14328.
- 55. Ishida, Y.; Shimada, T.; Ramasamy, E.; Ramamurthy, V.; Takagi, S. Room Temperature Phosphorescence from a Guest Molecule Confined in the Restrictive Space of an Organic–inorganic Supramolecular Assembly. *Photochem. Photobiol. Sci.*, **2016**, *15*, 959–963.
- 56. Porel, M.; Jayaraj, N.; Kaanumalle, L. S.; Maddipatla, M. V. S. N.; Parthasarathy, A.; Ramamurthy, V. Cavitand Octa Acid Forms a Nonpolar Capsuleplex Dependent on the Molecular Size and Hydrophobicity of the Guest. *Langmuir* **2009**, *25*, 3473–3481.
- 57. Kulasekharan, R.; Jayaraj, N.; Porel, M.; Choudhury, R.; Sundaresan, A. K.; Parthasarathy, A.; Ottaviani, M. F.; Jockusch, S.; Turro, N. J.; Ramamurthy, V. Guest Rotations within a Capsuleplex Probed by NMR and EPR Techniques. *Langmuir* **2010**, *26*, 6943–6953.
- 58. Das, A.; Sharma, G.; Kamatham, N.; Prabhakar, R.; Sen, P.; Ramamurthy, V. Ultrafast Solvation Dynamics Reveal the Octa Acid Capsule's Interior Dryness Depends on the Guest. *J. Phys. Chem. A* **2019**, *123*, 5928–5936.
- 59. Jayaraj, N.; Jockusch, S.; Kaanumalle, L. S.; Turro, N. J.; Ramamurthy, V. Dynamics of capsuleplex formed between octaacid and organic guest molecules Photophysical techniques reveal the opening and closing of capsuleplex. *Can. J. Chem.* **2011**, *89*, 203–213.
- 60. Nad, S.; Kumbhakar, M.; Pal, H. Photophysical Properties of Coumarin-152 and Coumarin-481 Dyes: Unusual Behavior in Nonpolar and in Higher Polarity Solvents, *J. Phys. Chem. A* **2003**, *107*, 4808-4816.
- 61. Yamaguchi, Y.; Matsubara, Y.; Ochi, T.; Wakamiya, T.; Yoshida, Z. How the π
 Conjugation Length Affects the Fluorescence Emission Efficiency. *J. Am. Chem. Soc.*2008, 130, 13867–13869.
- 62. Humbert-Droz, M.; Piguet, C.; Wesolowski, T.A. Fluorescence quantum yield rationalized by the magnitude of the charge transfer in p-conjugated terpyridine derivatives. *Phys. Chem. Chem. Phys.* **2016**, *18*, 29387.

TOC Graphics

